Enhancing the Detectability of Clouds and their Shadows in multitemporal Dryland Landsat Imagery: Extending Fmask

David Frantz[1*], Achim Röder[1], Thomas Udelhoven[1], Michael Schmidt[2,3]

Affiliations:
[1] Environmental Remote Sensing & Geoinformatics, Faculty of Spatial and Environmental Sciences, Trier University, 54296 Trier, Germany.
[2] Joint Remote Sensing Research Program, School of Geography, Planning and Environmental Management, University of Queensland, St Lucia, QLD 4072, Australia
[3] Department of Science, Information Technology and Innovation, 41 Boggo Rd, Dutton Park, QLD 4102, Australia

[*]Corresponding Author:
David Frantz, e-Mail: frantz@uni-trier.de

Reference:
D. Frantz, A. Röder, T. Udelhoven and M. Schmidt, "Enhancing the Detectability of Clouds and Their Shadows in Multitemporal Dryland Landsat Imagery: Extending Fmask," in *IEEE Geoscience and Remote Sensing Letters*, vol. 12, no. 6, pp. 1242-1246, June 2015.

DOI: 10.1109/LGRS.2015.2390673
Online available at: http://ieeexplore.ieee.org/xpl/articleDetails.jsp?arnumber=7035005

***Abstract*—We developed a new two-step approach for automated masking of clouds and their shadows in Landsat imagery. The first step is comprised of detecting clouds and cloud shadows in every Landsat image independently by using the Fmask algorithm. We modified two features of the original Fmask: we dropped the termination criterion for shadow matching and we appended a darkness filter to counteract false-positives in bifidly structured dryland areas. The second step utilizes the scene-by-scene detections of the first step and additional time series of cloud and cloud shadow probabilities. All clear-sky observations of a pixel are used to estimate the probabilities' median and standard deviation. Any observation that deviates more than a multiple of the standard deviation from the median is considered an outlier and thus a remaining cloud or cloud shadow. The method was specifically designed for use in water-limited dryland areas, where event-based precipitation is predominant. As an effect, green vegetation peaks are highly variable, both in timing, magnitude and frequency with adverse effects on commonly used Fourier-based outlier detection methods. The method is designed to be robust even if temporally dense data coverage is not available.**

***Index Terms*—Cloud detection, drylands, Landsat, multitemporal, remote sensing, time series.**

I. INTRODUCTION

LANDSAT data are one of the most valuable resources for earth observation [1]-[2], because of long term data continuity [3], free data access [4] and their optimal resolution to monitor landscape processes [5]. However, a great proportion of all available Landsat images is obscured by clouds and their shadows, most predominantly in the tropics [6].

The detection of clouds and their shadows is an inevitably required early step in any following image analysis application, because clouds adversely influence most analyses, among them atmospheric corrections, biophysical variables like the Normalized Difference Vegetation Index (NDVI [7]) values and land cover classifications [8].

Clouds either reduce the amount of usable data if cloud contaminated scenes are simply discarded or they have to be detected and masked. Historically, the overall cloud contamination of a Landsat scene was estimated by the Automated Cloud Cover Assessment (ACCA) system [9]-[10]. In general, ACCA fails to delineate the exact location and boundaries of clouds and their shadows [8] with adverse effects on automated analyses. Therefore, manual cloud detection was often performed, which in turn limited the amount of usable data, because of time and cost limitations.

Fortunately, cloud and cloud shadow detection in Landsat imagery has matured in the previous years with the development of the Fmask algorithm [8]. The accuracy of the Fmask results is reported to be good: [8] reported an overall accuracy of 96.41%, cloud producer's accuracy of 92.1% and cloud user's accuracy of 89.4%. The producer's accuracy for shadows is more than 70% and the user's accuracy is more than 50%. They used 142 manually screened reference images, globally stratified over 9 latitudinal zones.

The Fmask algorithm applies one scene-specific probability threshold for all pixels in a scene [8]. Cloud and cloud shadow masks can be further enhanced by applying time series based detection methods that make use of the scene-by-scene detections of Fmask. Besides other multi-temporal cloud detection approaches (e.g. [11]), [12]-[13] presented a subsequent time series analysis of TOA reflectance, developed in a rather humid study area in the Northeastern United States. They fit series of sine and cosine functions to the remaining clear-sky observations for each pixel and detect outliers (i.e. missed clouds and cloud shadows) using the model residuals.

Unlike temperate areas, water-limited dryland areas are often comprised of evergreen woodlands, open forests and grasslands that do not follow a strict sinusoidal phenological course. Phenology in arid areas is rather driven by event based precipitation [14] that is highly variable, both in timing, magnitude and frequency and can trigger a flush of (green) vegetation growth. In these cases, the conditions of equidistantly spaced phenology peaks is not met anymore and thus, fitting a Fourier based model of sine

and cosine functions might not be an appropriate choice [15]. Large data gaps are a general problem where either the acquisition plan or the cloud coverage do not permit a high frequent data coverage, e.g. areas outside the U.S., which were frequently not part of Landsat's acquisition plans. Although the current effort of reallocating data from foreign data providers [16] eases this drawback to a certain degree, temporal dense coverage is still an issue in many places. In addition, dryland biomes are often characterized by a pronounced partitioning of seasonality into a dry and wet season. During the wet season, where phenology is most dynamic, cloud-free Landsat data are often not available. Therefore, fitting a sine-based model might not be the best choice under these specific circumstances.

Here we present an approach to identify additional clouds and cloud shadows in Landsat imagery using a two-step cloud screening procedure, especially tailored for dryland ecosystems. The first step is comprised of applying the Fmask algorithm to the individual Landsat images [8]. We modified two criteria of the Fmask algorithm to perform better in a dryland environment. The second step is a subsequent time-series based outlier detection method, based on the results of the first step to reduce omission errors. It is designed as an alternative to the method presented by [13] for areas where the middle of the growing period(s) does not occur at the same time every year.

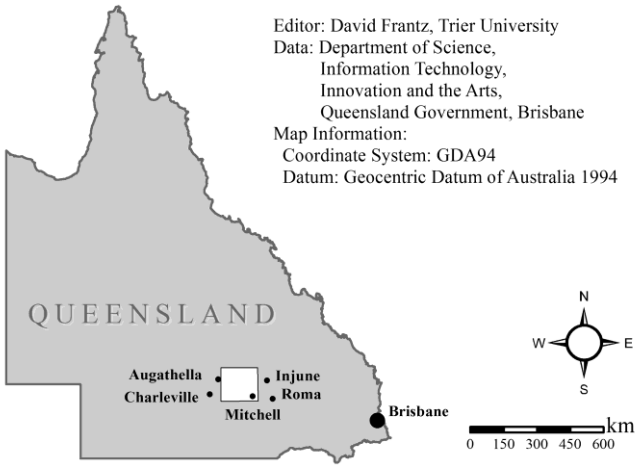

Fig. 1: Study Area.

II. STUDY AREA

The method was developed in an Australian savanna ecosystem in Queensland. The study area is included in WRS-2 Path/Row 093/078 and is centered at approximately 26°00’08’’S and 147°25’48’’E. The location of the study area (150 x 150 km) is displayed in Fig. 1 as the white box. The structural formations dominating the area, namely open forests and woodlands, are characteristic for Queensland's savannas, accounting for over 70 % of Australian forests in terms of structure and biomass [17]. The major tree communities in this area are formed by evergreen eucalyptus, acacia or callitris dominated woodlands to open forests (Regional Ecosystem Mapping of 2006 [18]). The region is characterized by variable rainfall and the ecosystem itself is generally water limited. The average monthly evaporation exceeds the average monthly rainfall throughout the year [19] with a pronounced dry and wet season, where the rainfall is precipitated by short duration storms with high temporal and spatial variability [19].

III. Data

All available Landsat-5 Thematic Mapper (TM) data of WRS-2 path/row 93/78 for the three year period of 2007-2009 were used in this study. Standard terrain corrected (Level 1T) Landsat data were obtained from the U.S. Geological Survey archive (USGS). Images that were not corrected to L1T precision were discarded, as a reliable co-registration among images was considered to be of major importance.

IV. Methods

The presented method is a two-step cloud screening procedure, where the first step is comprised of scene-by-scene detections with a slightly modified version of the Fmask algorithm [8]. The results from the first step are utilized in the second step, where the cloud and cloud shadow probabilities and the final masks are used in a time-series based outlier detection method.

A. Step 1: Fmask

Fmask is a fully automated cloud and cloud shadow screening application based on TOA reflectance [8]. Fmask is based on physical properties of clouds and their shadows to produce potential layers of clouds and cloud shadows. Cloud shadows are found by combining several existing approaches; i.e. object matching and lapse rate methods. The original algorithm is described in detail in [8]. Here we adapted the code in two major points to meet our requirements:

*1)*Termination criterion

In Fmask [8], shadows are matched by utilizing the geometrical relationship between a cloud and its shadow as well as modeling the three-dimensional shape and its presumed base height by using temperature information. This 3D shape is projected to the ground, while iterating through possible cloud base heights. For every iteration, a match similarity between the calculated shadow and a potential layer of shadows is computed. Iteration proceeds until the match becomes less than 98% of the maximum match similarity. We decided to discard this termination criterion. Shadow matching was found to terminate too early in many cases, which meant that only a fraction of the shadow was captured. In this implementation, the shadow match with the highest match similarity was considered the winner if the score was greater than 0.3. Otherwise no shadow was matched.

*2)*Darkness Filter

In the dryland ecosystems under investigation, we encountered a special case of land cover composition, where Fmask occasionally produced a high rate of false positives. This applies if the image is composed of two extremely different land cover classes with uneven areal distribution. Drylands are often comprised of very bright and hot surfaces (due to their sparse and dried-out vegetation cover), but in the presence of open water, patches of active vegetation can co-exist in the same image (e.g. river deltas, river basins and the like). These dark vegetation patches might be classified as clouds if the bright surface types are more dominant in terms of area.

During the selection of the PCPs (Potential Cloud Pixel), dark pixels might pass because the implemented Whiteness filter is rather a “Flatness” filter, which excludes pixels that have a high variability in the visible bands. Thus this filter also lets sufficiently black or grey pixels pass. We integrated an additional darkness filter into the PCP selection query (i.e. potentially cloudy only if the mean reflectance of the visible bands > 0.15). This filter is based on the observation that clouds are normally rather white.

Furthermore, the cloud probability of these features is usually very high because of the large temperature difference between the bright surrounding area and the vegetated surface. In Fmask, the temperature probability is derived by a quantile based approach that uses all non-PCP pixels. In the savanna systems under investigation, the bright and hot part of the image often dominates in terms of area, thus the temperature probability gets biased towards the hot surfaces. Water-cooled and

transpirating vegetated surfaces are then significantly colder and hence show a very high cloud probability. Therefore, the darkness filter was also added in the selection of the final cloud layer, where the cloud probability is otherwise the dominant driver to identify cloudy pixels.

In addition to the original Fmask implementation, the internal intermediate probability products, namely the cloud and cloud shadow probabilities are stored. Pixel-based time series of these probabilities are used to capture additional clouds and their shadows in the second step. A short description of the probability layers is presented in the following, details can be found in the original Fmask publication [8].

1)Cloud probability

In Fmask, the cloud probability is derived by combining land or water specific thematic probabilities. For both land and water, a temperature probability is estimated by rescaling the Brightness Temperature (BT) by percentiles of the land/water clear-sky pixels' BT. Various spectral tests are performed to obtain estimates of clear sky pixels in an early stage of the algorithm. In case of water, a brightness probability is computed. It exploits the property of water to have a very low, but stable reflectance in Band 5 and a significant increase in case of a cloud. Contrary, optical reflectance is very inconsistent for different land cover types, while being quite constant for clouds [8]. Thus a variability probability is computed instead of a brightness probability. The Whiteness Index [20] and modified versions of NDVI [7] and NDSI (Normalized Difference Snow Index [21]) are used to capture the earth land surface's spectral variability. Modified versions of NDVI and NDSI are used to counteract inconsistent index behavior in case of saturated VIS but under-saturated NIR and SWIR bands [22].

2)Shadow probability

Shadowed areas are mainly illuminated by scattered radiation and the scattering in NIR and SWIR bands is weaker than in VIS [23]. Additionally, NIR and SWIR reflectance is usually higher than the reflectance in VIS. Thus, a stronger darkening effect is evident in the long wavelength bands. Therefore, a morphological flood-fill transformation of bands 4 and 5 is performed in Fmask [24]-[25]. This filling procedure causes objects with a local depression in reflectance compared to their surroundings (e.g. cloud shadows, but also lakes or patches of vegetation in a desert) to be filled with the values along their border.

B. Step 2: Outlier detection

Once all individual images are processed with Fmask and the cloud and cloud probabilities are saved as second output product, we implemented a time series algorithm, which detects additional clouds and shadows on a per-pixel basis. The cloud and shadow masks are used to provide the clear-sky observations, whereas the probabilities are used to separate some remaining clouds and shadows from this data heap. Clear-sky observations are used to estimate basic statistics of the land surface. A deviation from these statistics is considered as cloud remnant. The process is illustrated as workflow in Fig. 2.

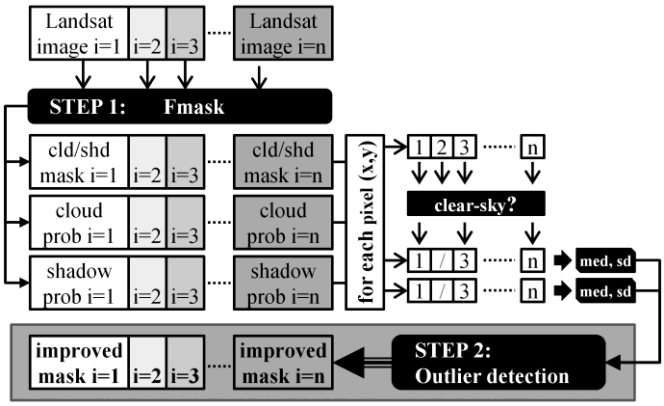

Fig. 2: Workflow of the two-step algorithm.

The probabilities of the clear-sky observations are assumed to be stable throughout time – at least for a restricted period of time. Therefore an anomaly in any of the probabilities throughout a three-year-period was considered as being an undetected cloud or cloud shadow. For each pixel *(x,y)*, the median and the standard deviation of the clear-sky time series are computed for each probability $prob_j$, with $j = \{cld, shd\}$. A pixel at time t_i, $i=1,\ldots,n$ (n = number of images) is marked as outlier if any $prob_j$ is greater than a threshold thr_j (eq. 1), which is its median plus a multiple m of its standard deviation (eq. 2). The multipliers m_j are the only tweakable input parameters of our algorithm. They allow for balancing the omission and commission errors. Ideally, they can be found by inverting the code with a Look-up-Table approach, where the parameters are chosen that match the best with an independent dataset. In practice, this might not be applicable due to problems in setting up a reference dataset of sufficient quality as outlined by [13]. Therefore, the choice of the multipliers m_j will be in practice based on visual scene analysis. For our presented data, we set m_{shd} to 3.5, m_{cld} was set to 3, though we suggest that these parameters should be reconsidered for every study site.

$$outlier(x,y,t_i) = prob_{cld}(x,y,t_i) > thr_{cld} \parallel prob_{shd}(x,y,t_i) > thr_{shd} \quad (1)$$

$$thr_j = med(prob_j(x,y)) + m_j \cdot sd(prob_j(x,y)) \quad (2)$$

This approach tends to identify many small outlier objects accidentally. Therefore, rigorous spatial filtering is applied to each mask image at times t_i. An outlier pixel is only accepted if it is completely surrounded by other outliers in an 8-connected neighborhood. If not, the outlier is rejected and considered to be clear-sky. Finally, all remaining outliers are buffered by 7 pixels and the outlier masks and original Fmask-derived masks are combined for each point in time *i*.

V. Results and Discussion

Fig. 3 illustrates the outlier method for two pixels (marked in Fig. 4) that were missed by Fmask. The outlier detection algorithm was capable of detecting data points within the shadow probability time series (a) and the cloud probability time series (b). In the case of the cloud probability example (b), the importance of the removal of Fmask identifications (yellow) for calculating the statistics is evident, where the inclusion of these data points could bias the standard deviation and the median (the effect on standard deviation might be more severe) in a way that the outlier would not be detected anymore. In addition, apparently the use of cloud and shadow probabilities allows us to use rather simple thresholding techniques compared to [13] as the probability layers are mostly free of phenological fluctuations. We superimposed the clear-sky NDVI time series in Fig. 3. It can be seen that there is an irregular, rainfall driven phenology, which is clearly visible in the NDVI, but not in the probability time series. The fluctuations in the probability time series are rather erratic and do not seem to inherit from phenological processes.

Furthermore, it can be seen that detecting clouds and shadows in this specialized data space allows even for the detection of thin clouds (example b), where the cloud is not even clearly visible in the NDVI transformation.

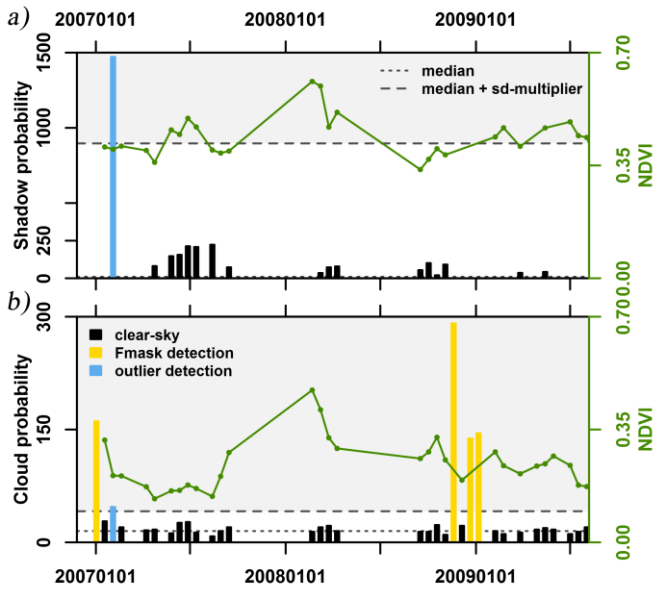

Fig. 3: Illustration of the time series outlier detection for two pixels marked in Fig. 4. An outlier (blue bars) is detected if its cloud/shadow probability is greater than the pixel median + a standard deviation multiplier (statistics retrieved from the clear-sky observations, black bars), thus being in the grey area. Fmask detections (yellow bars) are used to separate most of the observations before calculating the statistics. NDVI time series of the clear-sky observations are plotted in green.

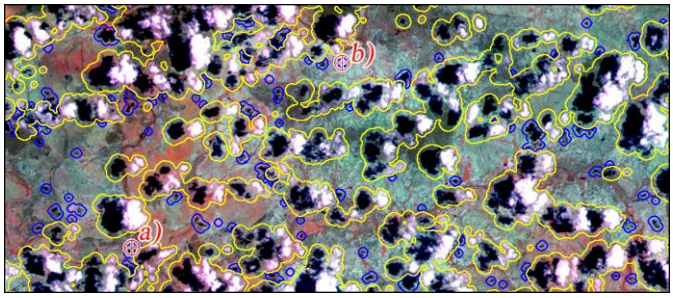

Fig. 4: Landsat RGB-composite (bands 4/5/3, i.e. NIR/SWIR1/RED) for the illustration of the outlier detection method (blue) as compared to the Fmask detections (yellow). The image was captured on 02/03/2007, which corresponds to the date with the blue bars in Fig. 3; the corresponding pixels are marked with a) and b).

Fig. 4 (a) depicts typical results of Fmask and of the extension for an example of a densely packed cumulus formation. Yellow polygons depict the Fmask results and additional outliers are drawn in blue. Especially cloud shadows are subject to omission in Fmask, which was to be expected as the shadow inaccuracy was determined to be higher [8]. This is particularly true in cases where the cloud was missed or the cloud is extremely cold and high and thus too far away to be linked properly to its shadow. Furthermore, small and almost transparent clouds were sometimes not detected, too (e.g. the cloud marked by b). Very thin stratus clouds or plumes of thick haze/high aerosols were also of concern (not depicted here). A high proportion of these objects could be captured with the additional outlier approach. The outlier detection produced reasonable results for most land cover types. As an exception, there were some false positives when dark objects of short duration were present. Fresh burn scars are characterized by a charred and dark surface, thus the shadow probability increases rapidly for a short time. Therefore, some recently burned areas were flagged partially as being shadow. We expect that this is also true for other transient dark

features (as temporal flooding), though we did not encounter this in our testing data. In a future version of our algorithm, we might account for this problem by exploiting the cloud/shadow geometry, e.g. by implementing another repeat of the Fmask shadow matching routine after the outlier detection step or by simply rejecting shadow detections that are too far away from the next cloud.

The time series based outlier detection in the probability images was designed to decrease the error of omission. The error of commission might increase to some degree or might remain unaffected. As a suggestion, this method can be used in applications that are very sensitive to remaining cloud contamination, but are robust in case of missing data. For example, STARFM (Spatial and Temporal Adaptive Reflectance Fusion Model [26]) predictions are very likely to decrease if transient changes in reflectance are present (e.g. clouds) and are per se designed to bridge temporal data gaps and make use of multiple images and neighborhood information. This means in most cases there will still be an estimated pixel value, even if that specific pixel was masked out in one image.

VI. Summary

Cloud and cloud shadow detection in Landsat imagery has matured recently with the introduction of Fmask [8]. Fmask accuracy is known to be of very high quality, though not perfect. Therefore, a two step cloud and cloud shadow screening method was introduced to decrease omission errors for applications that are sensitive to remaining cloud contamination. We modified two features of the original Fmask code (first step). Firstly, the termination criterion for shadow matching was dropped. Secondly, we added a darkness filter to improve detections for areas that are characterized by large surface property gradients.

A robust time series based outlier detection method was developed to reduce omission errors. The method utilizes the scene-by-scene detections of the first step. All clear-sky observations of a pixel are used to estimate the median and standard deviation of the cloud and cloud shadow probability time series. The cloud and cloud shadow probabilities are intermediate products of Fmask [8].

Contrary to existing add-ons [12]-[13] the presented algorithm was specifically developed for dryland areas that are characterized by the absence of phenology peaks at regular intervals. Furthermore, the algorithm is considered to be more robust in case of temporally sparse Landsat data and bad acquisition distributions over the year due to a pronounced dry/wet seasonality because of the conceptual simplicity. In addition, the method’s simplicity and its non-iterative nature might give it an edge compared to [13] if computation speed or access to high-end hardware is a limiting factor.

Acknowledgment

Landsat data courtesy of the U.S. Geological Survey. We like to thank Zhe Zhu & Curtis Woodcock for providing the Fmask code. We are grateful to two anonymous reviewers whose comments helped improve the manuscript.

REFERENCES

[1] Cohen, W.B. & Goward, S.N. (2004). Landsat's Role in Ecological Applications of Remote Sensing. BioScience, 54 (6), 535-545.

[2] Leimgruber, P., Christen, C.A., Laborderie, A. (2005). The Impact of Landsat Satellite Monitoring on Conservation Biology. Environmental Monitoring and Assessment, 106, 81-101.

[3] Wulder, M.A., White, J.C., Goward, S.N., Masek, J.G., Irons, J.R., Herold, M., Cohen, W.B., Loveland, T.R., Woodcock, C.E. (2008). Landsat Continuity: Issues and opportunities for land cover monitoring. Remote Sensing of Environment, 112, 955-969.

[4] Woodcock, C.E., Allen, R., Anderson, M., Belward, A., Bindschadler, R., Cohen, W., Gao, F., Goward, S.N., Helder, D., Helmer, E., Nemani, R., Oreopoulos, L., Schott, J., Thenkabail, P.S., Vermote, E.F., Vogelmann, J., Wulder, M.A., Wynne, R. (2008). Free Access to Landsat Imagery. Science, 320, 1011-1012.

[5] Danaher, T., Scarth, P., Armston, J., Collett, L., Kitchen, J., Gillingham, S. (2010). Remote Sensing of Tree-Grass Systems - the Eastern Australian Woodlands. In: Ecosystem Function in Savannas: Measurement and Modeling at Landscape to Global Scales, Hill, M.J. & Hanan, N.P. (Eds.), Taylor and Francis, 175-193.

[6] Asner, G.P. (2001). Cloud Cover in Landsat observations of the Brazilian Amazon. International Journal of Remote Sensing, 22 (18).

[7] Tucker, C.J. (1978). Red and Photographic Infrared Linear Combinations for Monitoring Vegetation. Remote Sensing of Environment, 8,127-150.

[8] Zhu, Z., Woodcock, C.E. (2012). Object-based cloud and cloud shadow detection in Landsat imagery. Remote Sensing of Environment, 118, 83-94.

[9] Irish, R. (2000). Landsat-7 automatic cloud cover assessment algorithms for multispectral, hyperspectral, and ultraspectral imagery. The International Society for Optical Engineering, 4049, 348–355.

[10] Irish, R., Barker, J.L., Goward, S.N., & Arvidson, T. (2006). Characterization of theLandsat-7 ETM+ Automated Cloud-Cover Assessment (ACCA) algorithm. Photogrammetric Engineering and Remote Sensing, 72 (10), 1179–1188.

[11] Hagolle, O., Huc, M., Villa Pascual, D., and Dedieu, G., A multi-temporal method for cloud detection, applied to FORMOSAT-2, VENμS, LANDSAT and SENTINEL-2 images. Remote Sensing of Environment, 114 (8), 1747–1755.

[12] Zhu, Z., Woodcock, C.E., Olofsson, P. (2012). Continuous monitoring of forest disturbance using all available Landsat imagery. Remote Sensing of Environment, 122, 75-91.

[13] Zhu, Z., Woodcock, C.E. (2014). Automated cloud, cloud shadow, and snow detection in multitemporal Landsat data: An algorithm designed specifically for monitoring land cover change. Remote Sensing of Environment, 152, 217-234.

[14] Tan, B., Morisette, J.T., Wolfe, R.E., Gao, F., Ederer, G.A., Nightingale, J., Pedelty, J.A. (2011). An Enhanced TIMESAT Algorithm for Estimating Vegetation Phenology Metrics From MODIS Data. IEEE Journal Of Selected Topics In Applied Earth Observations And Remote Sensing, 4 (2), 361-371.

[15] Mader, S. (2012). A Framework for the Phenological Analysis of Hypertemporal Remote Sensing Data Based on Polynomial Spline Models. PhD dissertation, Universität Trier, Germany. http://ubt.opus.hbz-nrw.de/volltexte/2012/783/

[16] Hansen, M.C., Loveland, T.R. (2012). A review of large area monitoring of land cover change using landsat data. Remote Sensing of Environment, 122, 66-74.

[17] Lucas, R.M., Cronin, N., Lee, A., Moghaddam, M., Witte, C., Tickle, P. (2006). Empirical relationships between AIRSAR backscatter and LiDAR-derives forest biomass, Queensland, Australia. Remote Sensing of Environment, 100, 407-425.

[18] Neldner, V.J., Wilson, B.A., Thompson, E.J., Dillewaard, H.A. (2012). Methodology for Survey and Mapping of Regional Ecosystems and Vegetation Communities in Queensland. Version 3.2. Queensland Herbarium, Department of Science, Information Technology, Innovation and the Arts, Brisbane, 124pp.

[19] Cowie, B.A., Thornton, C.M., Radford, B.J. (2007). The Brigalow Catchment Study: I. Overview of a 40-year study of the effects of land clearing in the brigalow bioregion of Australia. Australian Journal of Soil Research, 45, 479-495.

[20] Gomez-Chova, L., Camps-Valls, G., Galpe-Maravilla, J., Guanter, L., & Moreno, J. (2007). Cloud-screening algorithm for ENVISAT/MERIS multispectral images. IEEE Transactions on Geoscience and Remote Sensing, 45 (12), 4105–4118.

[21] Hall, D.K., Riggs, G.A., Salomonson, V.V. (1995). Development of methods for mapping global snow cover using moderate resolution imaging spectroradiometer data. Remote Sensing of Environment, 54, 127-140.

[22] Dozier, J. (1989). Spectral signature of alpine snow cover from the Landsat Thematic Mapper. Remote Sensing of Environment, 28, 9–22.

[23] Luo, Y., Trishchenko, A.P., & Khlopenkov, K.V. (2008). Developing clear-sky, cloud and cloud shadow mask for producing clear-sky composites at 250-meter spatial resolution for the seven MODIS land bands over Canada and North America. Remote Sensing of Environment, 112, 4167–4185.

[24] Soille, P., Vogt, J., Colombo, R. (2003). Carving and adaptive drainage enforcement of grid digital elevation models. Water Resources Research, 39 (12), 1366-1379.

[25] Vincent, L. (1993). Morphological Gayscale Reconstruction in Image Analysis: Applications and Efficient Algorithms. IEEE Transactions on Image Processing, 2 (2),176-201.

[26] Gao, F., Masek, J., Schwaller, M., Hall, F. (2006). On the blending of the Landsat and MODIS Surface Reflectance: Predicting Daily Landsat Surface Reflectance. IEEE Transactions on Geoscience and Remote Sensing, 44 (8), 2207-2218.